A Force-torque Sensor Based on a Stewart Platform in a Near-singular Configuration

R. Ranganath[*], P. S. Nair[†], T. S. Mruthyunjaya[‡], A. Ghosal[§]

Abstract

It is well known that a parallel mechanism at a singular configuration can gain one or more degrees of freedom instantaneously, and at such a configuration it cannot resist externally applied force/torque along certain directions. At near-singular configurations, small applied force/torque in a certain specific direction can give rise to large forces in the links, thereby resulting in mechanical magnification in link forces. This key idea is used, with a Stewart Platform, in a near-singular configuration, to design a directionally sensitive force-torque sensor. The concept of near-singular configuration and magnification is developed analytically and numerically with the help of a simple planar truss with rotary and flexure joints. A finite element analysis shows that a properly designed flexure joint approximates a rotary joint reasonably well, thus avoiding friction and non-linearities associated with rotary joints. The concept of force magnification and flexural joints is next extended to a Stewart Platform at a near-singular configuration. It is verified, using finite element analysis, that the Stewart Platform at a near-singular configuration with flexural hinges shows large forces in the legs for small external forces and torques applied in certain directions, and thus can be a good design for a highly sensitive force-torque sensor for certain components of applied force/torque. It is also shown, from a singularity analysis of the Stewart Platform, that sensitivity to other components of external force/torque can be obtained by using different near-singular configurations. The theoretical concepts are demonstrated with a prototype sensor which is sensitive to two components of the externally applied force and one component of the externally applied moment.

Keywords: Stewart Platform, singular configurations, force-torque sensor, flexure hinges.

1 Introduction

The Stewart Platform, originally proposed for a flight simulator by Stewart[1] has been suggested for a variety of applications (see, for example, Hunt[2], Fichter[3], Portman et al.,[4]). Several researchers have also proposed the use of a Stewart Platform as a six component force-torque sensor (see for example, Gaillet and Reboulet[5], Rees[6], Kerr[7], Nguyen et al.,[8], Romiti and Sorli[9], Sorli and Zhmud [10]). Hongrui et al.,[11] and Dasgupta et al., [12] proposed a Stewart Platform in an isotropic configuration where the sensor is equally sensitive to all directions of

[*]Spacecraft Mechanisms Group, ISRO Satellite Centre, Bangalore, email: rrrr@isac.ernet.in

[†]Structures Group, ISRO Satellite Centre, Bangalore, email: psnair@isac.ernet.in

[‡]Dept. of Mechanical Engineering, IISc., Bangalore, email: tsmru@yahoo.com

[§]Corresponding Author, Dept. of Mechanical Engineering, Indian Institute of Science, Bangalore – 560 012, India, email: asitava@mecheng.iisc.ernet.in

applied force-torque. Six axis force-torque sensors not based on Stewart Platform have also been proposed (see, for example, Hirose and Yoneda[13] and Hirzinger and Dietrich[14]). In a Stewart Platform manipulator, the legs are connected to the fixed base and moving platform by universal and spherical joints respectively. In a flight simulator or robotic applications, the leg lengths can be changed in a desired manner to achieve arbitrary motion of the platform. In a sensor application, the forces experienced by the legs due to the application of the external load needs to be measured (sensed) as accurately as possible. Typically, the force in the leg is measured in the form of strain and a strain sensing element such as strain gage is used. Dwarakanath et al.,[32] report the usage of ring shaped sensing element in the Stewart Platform sensor built by them. Abe et al., [16] propose a 'H' slit beam to achieve a sensitive unidirectional deformation for the measurement of small force/torques with overload protection. In a sensor application, the friction, backlash and other non-linearities at the passive spherical/universal joints of the Stewart Platform will affect the measurements in unpredictable ways. To avoid friction and backlash, researchers have proposed the use of flexural hinges. The basic theory of flexible hinges was given by Paros and Weisbord[15], and McInroy and Hamann[17] have proposed the use of flexural hinges for micro-manipulation. Zhang and Fasse[18] present a finite element based method to determine the stiffness properties of a notch hinge. Champagne et al.,[19] describe the design, fabrication, testing and operation of a six axis force and torque dynamo-meter where the support struts are provided with flexures for two axes, with one flexure for each axis, separated by a small distance to ensure adequate longitudinal stiffness.

As can be seen from the literature survey, the use of Stewart Platform as a sensor is aimed towards achieving an isotropic configuration. The goal in such a configuration is to achieve approximately equal sensitivity for all components of the applied external force-torque. Our goal is very different – we aim to design a Stewart Platform based force-torque sensor at a near-singular configuration[1]. In such a configuration, as we show in this paper, the forces in the legs will be large for small external forces/moments and thus can be sensed easily. Our main motivation for designing such force-torque sensors comes from applications such as robotic assembly and manufacturing where it is known that the forces in the normal directions are 5 to 10 times larger than in the tangential directions[34]. In addition, it is also well known in aerodynamics that the drag forces, pitching and other moments are typically 10 to 20 times smaller than lift forces. In such applications a sensor with enhanced sensitivity along certain directions will be useful. It may be noted that in *other directions* the sensitivity will be that of a normal load sensor determined by the sensitivity of the sensing element and the associated electronic amplification, and we can sense *all* the six components of the force and torque. The enhanced sensitivity, in selected directions, is *independent* of the sensitivity obtained through the use of sophisticated electronics in any sensor design. Indeed one can easily use our concept of magnification along specifically selected direction *together* with advanced electronics to take advantage of both. This concept is one of the key contributions of the paper.

To obtain high sensitivity in other set of desired directions, we can use different singular configurations. In this paper, we present an algorithm to compute *symbolically* the singular directions of

[1]Singularities of serial and parallel manipulators have been extensively studied (see, for example, [20, 28, 27] and the references therein). For a discussion on quantification of *near-singularity* see section 3.

a $6-6$ Stewart Platform and present a list of several configurations and their singular directions. This is also a contribution of this paper.

We demonstrate, by means of extensive finite element analysis, that the magnification of the forces in the legs is achieved even when the joints connecting the legs to the base and platform are replaced by flexural hinges. We show that there is a good agreement between the numerical results obtained by solving the Stewart Platform statics with spherical joints and the results obtained by replacing spherical joints with flexural hinges. Extensive numerical analysis is used to fine tune the design of a prototype sensor sensitive to two components of externally applied force and one component of externally applied moment. The numerical simulations clearly show that small perturbations of the geometry parameters, which may arise out of manufacturing tolerances, *do not* significantly affect the basic concept of magnification along specific directions. This is the third contribution of this paper.

Finally, we present a complete design of a force-torque sensor based on our ideas. The design includes a sensing element in the leg with inbuilt protection for biaxial bending for the flexural hinges. We present experimental results from a fabricated prototype sensor which clearly demonstrate the concept of higher sensitivity for external loads along specific directions.

This paper is organized as follows: in section 2, we develop the concept of magnification of forces in the links of a mechanism, in a near-singular configuration, with the help of a simple planar truss. In section 3, we extend the concepts, developed in section 2, to a spatial Stewart Platform. In section 4, numerical results with Stewart Platform, in a near-singular configuration, with spherical joints and flexure hinges are presented and discussed. In section 5, we present a design of the sensing element in the leg and an FEA of the complete Stewart Platform sensor with sensing element and flexural hinges. In section 6, we present calibration and experimental results from a prototype Stewart Platform sensor. Finally, in section 7, we present the conclusions of this paper.

2 Analysis of a planar truss

The figure 1 shows a planar truss with hinges at A and B fixed to the ground and the sides AC equal to BC. The truss members are assumed to be rigid. It is well known that for any θ not equal to zero degree and non-zero d, the configuration is a structure with zero degree of freedom. If a force F is applied at the hinge C, at an angle ϕ to the horizontal, the axial forces in the links AC and BC, denoted by R_1 and R_2 respectively, can be obtained from,

$$\begin{pmatrix} \cos\theta & -\cos\theta \\ \sin\theta & \sin\theta \end{pmatrix} \begin{pmatrix} R_1 \\ R_2 \end{pmatrix} = F \begin{pmatrix} \cos\phi \\ \sin\phi \end{pmatrix} \tag{1}$$

Denoting the matrix on the left-hand side by $[H]$, we note that for θ not equal to zero, the matrix $[H]$ is invertible and we can obtain R_1 and R_2 as

$$\begin{pmatrix} R_1 \\ R_2 \end{pmatrix} = [H]^{-1} \begin{pmatrix} F\cos\phi \\ F\sin\phi \end{pmatrix} = \frac{F}{2} \begin{pmatrix} \cos\phi/\cos\theta + \sin\phi/\sin\theta \\ -\cos\phi/\cos\theta + \sin\phi/\sin\theta \end{pmatrix} \tag{2}$$

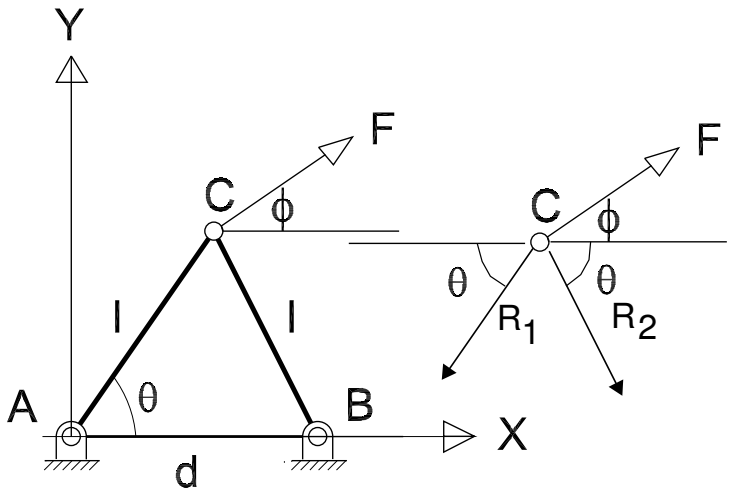

Figure 1: A planar two link hinged truss

When $\theta \to 0$ and $\phi \neq 0$, $\sin\theta \to 0$ and the axial forces R_1 and R_2 tend to infinity. At $\theta = 0$, the structure is in a singular configuration and it *gains* an instantaneous degree of freedom [20, 21]. The hinge C can move instantaneously along Y axis even for infinitely small F. For $\theta = 0$ and $\phi = 0$, the axial forces in the links are finite with $R_1 = -R_2 = F/2$. In terms of the eigenvalues of $[H]$, we note that for $\theta = 0$ and $\phi \neq 0$, the eigenvalues are 1 and 0. The eigenvector corresponding to 0 eigenvalue, mapped by $[H]$, is along the Y axis. This is the singular direction for the planar truss and the structure cannot withstand any force applied in the singular direction at $\theta = 0$.

Consider now that the links AC and BC are equipped with force sensing elements (strain gauge for example), and a force F is applied along Y axis ($\phi = \pi/2$) and θ *is non-zero but small.* From equation (2), we observe that the magnitude of R_1 and R_2 are $F/(2\sin\theta)$ and hence will be large even for a very small applied F – the sensing element can sense a very small applied force F. The sensitivity falls off as θ increases and also if the direction of the external force F tends toward horizontal. If the applied force is horizontal ($\phi = 0$) then there is no magnification, and the magnitude of R_1 and R_2 is $F/2$. The upper plot in figure 2 shows a plot of the magnification, $|R_1|/F$, with varying θ, and at $\theta = 1°$, the magnification is about 28.6. It may be noted that the magnification is nonlinear.

Next consider the links AC and BC to be *elastic*, and a force F is applied along Y axis ($\phi = \pi/2$). As the links are elastic, they will extend when an axial force is applied and as a result the angle θ will be modified. The new angle, θ_{new}, for a given θ is $\theta_{new} = \arctan(\delta + \delta_1)$[22], where, $\delta = l\sin\theta$ and $\delta_1 = l\cos\theta \times (F/EA)^{1/3}$ with l as the nominal length of the link, E as the Young's modulus, A as cross-sectional area and a Poisson's ratio of 0.3. The axial forces in the elastic links are now $R_1 = -R_2 = F/(2\sin\theta_{new})$. The variation of the magnification in link forces, considering the elasticity of the links, is shown in the lower plot in figure 2. In the plot, E is assumed to be 112000 N /mm^2, and A and l are assumed to be 7.068 mm^2 and 50 mm respectively. It is observed that for $\theta = 1°$, with the links considered as elastic, the magnification is approximately 21 as against 28.6 obtained for the rigid link case. The above concept of magnification at near-singular configuration

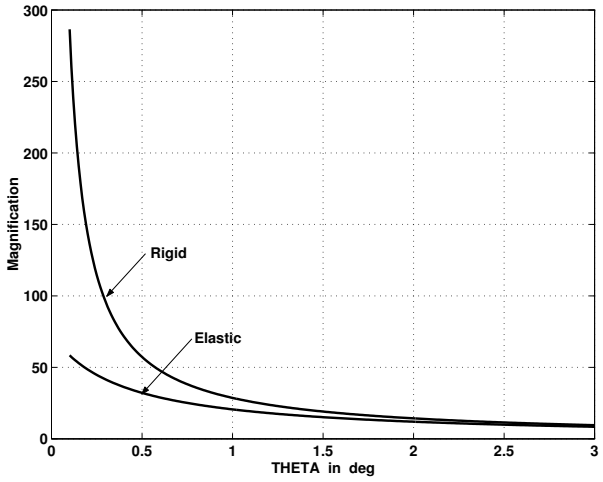

Figure 2: Magnification in axial force in the link as a function of θ

is one of the key ideas of this paper and is extended, in subsequent sections, for the design of a force-torque sensor sensitive along pre-determined directions.

2.1 Replacing joints by flexure hinges

The above analysis of the magnification of forces in the links was based on frictionless joints which allows the forces in the links AC and BC to be purely axial (tension or compression). In practice, any joint has friction, backlash and other non-linearities which will modify the axial forces in unpredictable ways. To avoid these problems, flexural hinges have been used in many applications such as gyroscopes, accelerometers, missile control nozzles and governors. For the sake of completeness, we briefly present the theory of flexural hinges by following the development in Paros et al.,[15].

A typical flexure hinge is shown in figure 3a which also shows the dimensions, various forces and moments which cause deflections in the flexure hinge. A simple two axes flexure hinge with intersecting axes is formed by necking down a round bar as shown in figure 3b. The expressions for angular compliances, for the flexure hinge shown in figure 3b, are given by[15],

$$\begin{aligned} \frac{\theta_y}{M_y} &= \frac{\theta_z}{M_z} = \frac{20R^{1/2}}{Ed^{7/2}} \\ \frac{\theta_y}{F_z} &= \frac{\theta_z}{F_y} = 20(\sqrt{2\gamma - \gamma^2})\frac{R^{3/2}}{Ed^{7/2}} \end{aligned} \tag{3}$$

where F_x, F_y and F_z are the forces acting along the X, Y and Z axes of the flexure hinge, M_y and M_z are the moments acting about the Y and Z axes, θ_y and θ_z are the corresponding angular deformations about Y and Z axes respectively, R is the radius, d is the minimum diameter, and E is the Young's modulus of the flexure hinge material. The quantity, γ, is the ratio of flexure hinge height, h, to twice the flexure hinge radius, R for the hinge in figure 3a. For the hinge in figure

3b, γ is the ratio of the diameter D with R. The expression for the longitudinal compliance for the hinge given in figure 3b by[15] is,

$$\frac{\delta_x}{F_x} = \frac{2R^{1/2}}{Ed^{3/2}} \tag{4}$$

where δ_x is the linear deformation along the X axis for the applied force F_x.

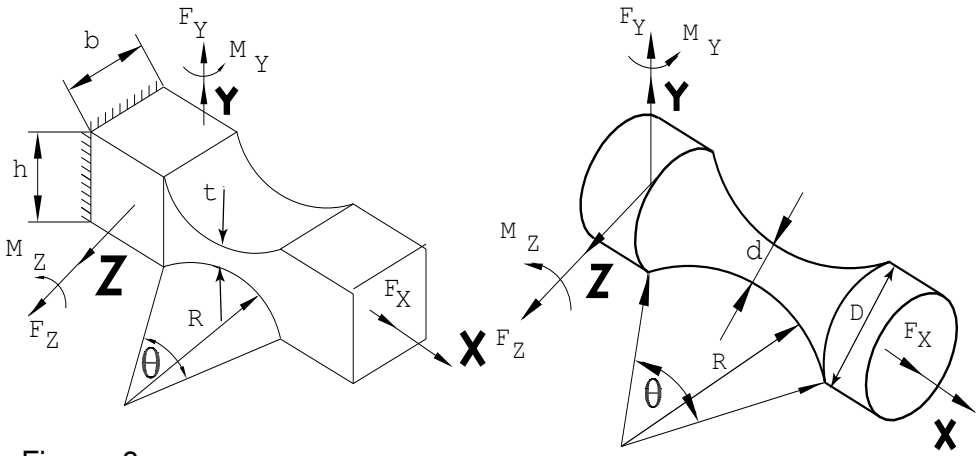

Figure 3: Flexure hinges

The above expressions are approximate and are estimated to be accurate within 1% of the actual value. It is seen from equations (3), that the angular compliances become large as the diameter d of the necked region reduces, and approximates a two axes hinge for small d. At the same time, from equation (4), the longitudinal compliance also increases with decrease in d. However, the longitudinal compliance is proportional to $d^{-3/2}$ whereas the angular compliance is proportional to $d^{-7/2}$. Hence, a careful choice of d is required to obtain acceptable angular compliance and, at the same time, an acceptable stiffness in the longitudinal direction. We can thereby obtain a flexible hinge which will approximate to a spherical joint undergoing small angular displacements without the disadvantages of friction and backlash associated with a practical spherical joint.

2.2 Numerical analysis of planar truss

We replace the rotary joints in the planar truss with flexural hinges. The link diameter is reduced (kinked) to d at the place of the joints, A and B (refer figure 1). The modeling was done in the software package NISA[23], for a truss of angle θ equal to 1° with the link meshed with 10 beam elements and the smaller diameter region with a finer mesh of 10 elements. The link lengths AC and AB are 50 mm each with diameter as 3 mm and reduced to d at the kink. The length of the beam kinked at the supports is 1 mm. The boundary conditions at A and B are assumed to be fixed with displacements $U_x = U_y = U_z = 0$ and rotations $R_x = R_y = R_z = 0$. For a force of 0.98 N, applied at the point C (modeled as a rotary joint using the end-release option in NISA [23]) along the Y axis, the axial force at a node near the middle of link AC are obtained as 8.7211 N, 9.9375

N, 19.3251 N, and 26.7813 N for kink diameters of 3 mm, 2 mm, 1 mm, and 0.5 mm respectively. It can be seen, that as kink diameter reduces the axial forces in the links approach the value of 28 N obtained from equation (2) with $\theta = 1^\circ$ and $\phi = \pi/2$. For a kink diameter of 0.5 mm, the error between the axial forces obtained from FEA and from equation (2) in the link AC is about 2.5%. It was also verified (see [24] for details) that the transverse forces and moments become smaller as the kink diameter reduces and the kinking is effective when θ is small, i.e., near-singular configurations. It may be noted that we cannot reduce d to arbitrary small values, since the material may undergo permanent deformation and this aspect has to be addressed during design.

3 Statics of a Stewart Platform

The Stewart Platform, as shown in figure 4, consists of six extensible legs (with prismatic joints in each leg) connected to the (moving) platform and (fixed) base with spherical(S) joints[2]. In a general configuration, the Stewart Platform has six active degrees-of-freedom and by actuating the six prismatic joints one can achieve arbitrary position and orientation of the moving platform. If an external force-moment is applied at the platform, we can obtain the *axial* forces in the legs required to keep the Stewart Platform in equilibrium. This forms the topic of the statics of the Stewart Platform and is well known (see, for example, Dasgupta et al .,[12]), and we present it in brief for completeness. Figure 4 shows a $6-6$ Stewart Platform manipulator with the fixed base frame located at the point $\mathbf{B}_0$, and a point $\mathbf{P}_0$ on the moving frame is located by the vector $\mathbf{t}$ from $\mathbf{B}_0$ (refer figure 5). The orientation of the moving platform with respect to the base frame is described by the rotation matrix $[R]$. The base connection points, $\mathbf{B}_i,\ i = 1, 2, .., 6$, are located by the vectors $\mathbf{b}_i,\ i = 1, 2, ..., 6$, with respect to the base frame and top connection points, $\mathbf{P}_i,\ i = 1, 2, .., 6$, are located with respect to the moving frame by vectors $\mathbf{p}_i,\ i = 1, 2, ..., 6$. Figure 5 shows an arbitrary i^{th} leg and the vectors $\mathbf{b}_i$, $\mathbf{p}_i$ and $\mathbf{t}$. The figure 5 also shows the prismatic joint whose translation along the leg vector $\mathbf{S}_i$ is denoted by l_i. The vector $\mathbf{p}_i$ can be written in the base frame as

$$(\mathbf{p}_i)_{\text{Base}} = [R]\mathbf{p}_i + \mathbf{t} \tag{5}$$

The leg vector can be written as

$$\mathbf{S}_i = [R]\mathbf{p}_i + \mathbf{t} - \mathbf{b}_i \tag{6}$$

We define a unit vector $\mathbf{s}_i = \mathbf{S}_i/l_i$ along which the prismatic joint can exert axial force f_i. The resultant force $\mathbf{F}$ and moment $\mathbf{M}$ that can be obtained by the application of $\mathbf{f}_i$'s are given by

$$\begin{aligned} \mathbf{F} &= \sum_{i=1}^{6} f_i \mathbf{s}_i \\ \mathbf{M} &= \sum_{i=1}^{6} f_i (\mathbf{b}_i \times \mathbf{s}_i) \end{aligned} \tag{7}$$

[2]To avoid passive rotation about the line joining the spherical joints, the S-P-S structure is replaced with a U-P-S structure in practical Stewart Platforms.

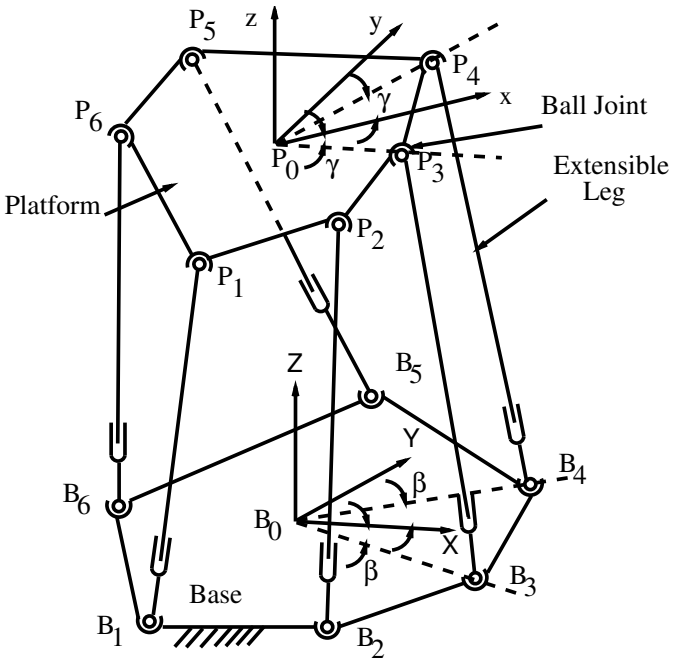

Figure 4: A $6-6$ Stewart Platform

The above equations can be written in a compact matrix form as

$$\begin{pmatrix} \mathbf{F} \\ \mathbf{M} \end{pmatrix} = [H]\mathbf{f} \tag{8}$$

where the matrix $[H]$ is given by

$$[H] = \begin{pmatrix} \mathbf{s}_1 & \mathbf{s}_2 & \mathbf{s}_3 & \mathbf{s}_4 & \mathbf{s}_5 & \mathbf{s}_6 \\ \mathbf{b}_1 \times \mathbf{s}_1 & \mathbf{b}_2 \times \mathbf{s}_2 & \mathbf{b}_3 \times \mathbf{s}_3 & \mathbf{b}_4 \times \mathbf{s}_4 & \mathbf{b}_5 \times \mathbf{s}_5 & \mathbf{b}_6 \times \mathbf{s}_6 \end{pmatrix} \tag{9}$$

The matrix $[H]$ is called the force transformation matrix and is similar in concept to the $[H]$ derived for the simple planar truss in the last section, and is also same as the transpose of the Jacobian matrix, $[J]$, used in velocity analysis of the Stewart Platform manipulator. The matrix $[H]$ maps the axial leg forces, $(f_1, f_2, ..., f_6)^T \in \mathcal{F} \subseteq \mathbf{R}^6$, applied to keep the Stewart Platform in static equilibrium, to the externally applied force/moment pair or wrench[3], $(\mathbf{F}; \mathbf{M})^T \in \mathcal{W} \subseteq \mathbf{R}^3 \times \mathbf{R}^3$. Similar to the planar truss, if $\det[H] = 0$ and the matrix $[H]$ is singular, some component(s) of the externally applied $\mathbf{F}$ and $\mathbf{M}$ cannot be supported by the structure (the Stewart Platform with the prismatic joints locked has zero degrees of freedom) and the structure gains one or more

[3]The pair $(\mathbf{F}; \mathbf{M})$ is strictly *not* an element of a vector space - they represent a force/moment pair acting at a point in a rigid body, and, in fact, the two parts have different units. Wrenches, along with screws and motors have been extensively studied in theoretical kinematics (see, for example, [29, 2, 30]).

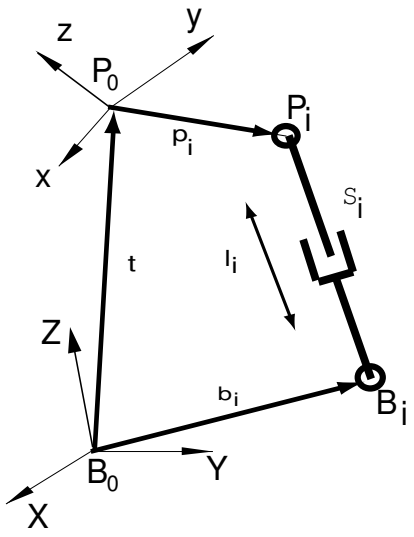

Figure 5: A typical leg of a $6-6$ Stewart Platform

degrees of freedom instantaneously. The eigenvectors corresponding to the zero eigenvalues of $[H]$ when mapped to $\mathcal{W}$ give the singular directions, and the Stewart Platform cannot withstand any force/moment applied along the singular directions. Again, if the Stewart Platform is in a *near-singular configuration*, then a *small non-zero* force/moment acting along the singular direction will lead to *large axial force* in one or more of the legs, and we will get large magnification.

In this paper, the key concept of *near-singular configuration* is quantified by the *condition number* of the matrix $[H]$ which is defined to be the ratio of the absolute value of the largest to the absolute value of the smallest eigenvalue of $[H]$. The condition number is infinity when the matrix is singular and 1.0 when the matrix is isotropic. It may be noted that the condition number of $[H]$ depends on the units chosen for the length parameters as the bottom 3×6 portion of $[H]$ depends on the choice of length units. In the numerical example in section 4, and in our nominal design, we choose parameters such that the *condition number* of $[H]$ is approximately 2000 with *mm* as length unit. This is found to give significant magnification along selected directions, and the matrix $[H]$ can still be accurately inverted. In addition, as discussed in section 4, around this condition number, the variation in condition number is also found to be not very large, and hence the magnification does not change significantly due to small changes in geometry.

In the next sub-section, we present an algorithm to obtain singular directions for a Stewart Platform and present singular directions for a few configurations.

3.1 Singular directions of a Stewart Platform

Consider a $6-6$ Stewart Platform with platform of same size as the base with both of them as regular hexagons. Consider also the case when the legs of the Stewart Platform are all parallel. In

such a case, the $[H]$ matrix is given by

$$[H] = \begin{pmatrix} 0 & 0 & 0 & 0 & 0 & 0 \\ 0 & 0 & 0 & 0 & 0 & 0 \\ 1 & 1 & 1 & 1 & 1 & 1 \\ b_{1_y} & b_{2_y} & b_{3_y} & b_{4_y} & b_{5_y} & b_{6_y} \\ -b_{1_x} & -b_{2_x} & -b_{3_x} & -b_{4_x} & -b_{5_x} & -b_{6_x} \\ 0 & 0 & 0 & 0 & 0 & 0 \end{pmatrix} \tag{10}$$

where the vector $\mathbf{b}_i$ locating the base points is given by $(b_{i_x}, b_{i_y}, b_{i_z})^T$, $i = 1, 2, ..., 6$. The above $[H]$ clearly has rank 3 and three eigenvalues are zero. For this $[H]$, it is intuitively clear that forces along X and Y axes cannot be resisted and likewise the moment along Z axis cannot be resisted. Hence, the singular directions in the $(\mathbf{F}; \mathbf{M})^T$ or $\mathcal{W}$ space are $(1, 0, 0; 0, 0, 0)^T$, $(0, 1, 0; 0, 0, 0)^T$, and $(0, 0, 0; 0, 0, 1)^T$. These intuitive singular directions also follow from the fact that the eigenvectors corresponding to the zero eigenvalues of $[H]$ map to directions $(1, 0, 0; 0, 0, 0)^T$, $(0, 1, 0; 0, 0, 0)^T$ and $(0, 0, 0; 0, 0, 1)^T$.

In general the above intuitive approach cannot be used for arbitrary configurations of Stewart Platform. We can always obtain the number of zero eigenvalues (or rank) of $[H]$ but it is not clear which of these give rise to force singularities and which give rise to moment singularities. It is also not possible to investigate numerically, since the matrix $[H]$ is singular and inversion to obtain leg forces (to check for magnification) for an applied external force or moment is not possible. To obtain singular directions, for arbitrary $6-6$ Stewart Platform configurations, we proceed as follows:

We observe from equation (8) and (9) that the external force, $\mathbf{F}$, can be written as

$$\mathbf{F} = [H_f]\mathbf{f} = \begin{bmatrix} \mathbf{s}_1 & \mathbf{s}_2 & \mathbf{s}_3 & \mathbf{s}_4 & \mathbf{s}_5 & \mathbf{s}_6 \end{bmatrix} \mathbf{f} \tag{11}$$

The square of the magnitude of $\mathbf{F}$ can be obtained by taking the dot product with itself, and denoting $[H_f]^T[H_f]$ by $[g_f]$, we can write

$$\mathbf{F}^T\mathbf{F} = \mathbf{f}^T[g_f]\mathbf{f} \tag{12}$$

The maximum, intermediate and minimum values of $\mathbf{F}^T\mathbf{F}$ subject to a constraint of the form $\mathbf{f}^T\mathbf{f} = 1$ are the eigenvalues of $[g_f]$ and since the rank of $[g_f]$ is 3 ($[H_f]$ has at most rank 3), we can show that the tip of the force vector, $\mathbf{F}$ lies on an ellipsoid in $\mathbf{R}^3$. The axes of the ellipsoid are along the *principal* forces and these can be obtained by mapping the eigenvectors corresponding to the non-zero eigenvalues of $[g_f]$ by $[H]$. It may be noted that since $[g_f]$ has maximum rank 3, three eigenvalues are always zero and the eigenvectors corresponding to these zero eigenvalues when mapped by $[H]$ give the principal moments (see [31]) at the origin. Mathematically, the six eigenvectors of $[g_f]$, arranged column-wise as matrix, $[X]$, after mapping by $[H]$ give the principal wrenches. We can write,

$$[H][X] = \left(\begin{array}{c|c} [0] & [F]^* \\ \hline [M]_o{}^* & [M]_p{}^* \end{array}\right) \tag{13}$$

where [0] is 3×3 matrix of zeros, $[F]^*$ is a 3×3 of principal forces, $[M]^*_o$ is a 3×3 matrix of principal moments at the origin, and $[M]^*_p$ is a 3×3 matrix of principal moments at centre of platform.

If the rank of $[g_f]$ is less than three, the force ellipsoid shrinks to an ellipse, a line or a point[4]. The singular directions of force can be obtained by mapping the eigenvectors corresponding to the zero eigenvalues of $[g_f]$ or by obtaining the null space of $[F]^*$. Likewise the singular directions of the moments is the null space of $[M]^*_o$. It may be noted that the sub-matrix $[M]^*_p$ depends on the point of application of the moment whereas $[M]^*_o$ contains the principal moments at the origin and is more relevant in our discussion.

We summarize the above discussion in the form of an algorithm to obtain force and moment singular directions in $6-6$ Stewart Platforms.

Algorithm to obtain singular direction(s) in $6-6$ Stewart Platforms

- Enumerate all possible $6-6$ Stewart Platforms by choosing pairs of base and platform points (a few of them are shown in Table 1). For each of the configurations,
  - Compute the number of zero eigenvalues of $[H]$. This will give the total number of singular directions *including* force and moments.
  - Obtain all eigenvalues and corresponding eigenvectors *symbolically* for $[g_f]$ using a symbolic manipulation package.
  - Obtain the matrix $[H][X]$ and sub-matrices $[F]^*$ and $[M]^*_o$ (see equation (13)).
  - Obtain null space vectors of $[F]^*$ and $[M]^*_o$ to obtain the singular force and moment directions (if any).

The above algorithm and the computations were performed symbolically using the software package Mathematica[26] for various configurations of $6-6$ Stewart Platforms and the results showing singular force and moment directions for several Stewart Platform configurations are presented in Table 1. It may be noted that the singular directions need not be always along X, Y or Z axis – in configurations 6, 11, 14 and 18, the singular force direction is in the $X-Y$ plane. It can be also noted that none of the configurations give force singular directions along Z axis although all other directions are possible. It was found after extensive search that to obtain F_z, we have to make $\mathbf{t}$, the distance between the base and platform as $\mathbf{0}$. This means that the base and the platform are in the same plane and hence this is not a feasible configuration for sensor design. It is possible to get a force singular direction in the $X-Z$ plane by translating the platform horizontally in configuration No. 1 (see Table 1). In particular for $\mathbf{t} = 100(1,0,1)^T$, the singular force directions are along $(1/\sqrt{2})(-1,0,1)^T$ and $(0,1,0)^T$ and the singular moment direction is $(1/\sqrt{2})(1,0,1)^T$.

[4]This is similar to the concepts of singularities of point trajectories discussed in [27].

Table 1: Singular directions of Stewart Platform configurations

	Leg Connections						'0' Eig. Val	Singular
No.	Leg 1	Leg 2	Leg 3	Leg 4	Leg 5	Leg 6	of $[H]$	Directions
1	B_1-P_1	B_2-P_2	B_3-P_3	B_4-P_4	B_5-P_5	B_6-P_6	3	F_x, F_y, M_z
2	B_1-P_2	B_2-P_1	B_3-P_3	B_4-P_4	B_5-P_5	B_6-P_6	2	F_x, M_z
3	B_1-P_2	B_2-P_1	B_3-P_4	B_4-P_3	B_5-P_5	B_6-P_6	1	M_z
4	B_1-P_2	B_2-P_1	B_3-P_4	B_4-P_3	B_5-P_6	B_6-P_5	0	none
5	B_1-P_1	B_2-P_3	B_3-P_2	B_4-P_5	B_5-P_4	B_6-P_6	1	M_z
6	B_1-P_3	B_2-P_2	B_3-P_1	B_4-P_4	B_5-P_5	B_6-P_6	2	$M_z,[\frac{1}{\sqrt{9}},1,0]^1$
7	B_1-P_3	B_2-P_4	B_3-P_1	B_4-P_2	B_5-P_5	B_6-P_6	1	M_z
8	B_1-P_3	B_2-P_4	B_3-P_1	B_4-P_2	B_5-P_6	B_6-P_5	0	none
9	B_1-P_4	B_2-P_2	B_3-P_3	B_4-P_1	B_5-P_5	B_6-P_6	2	F_y, M_z
10	B_1-P_4	B_2-P_5	B_3-P_6	B_4-P_1	B_5-P_2	B_6-P_3	3	M_x, M_y, M_z
11	B_1-P_5	B_2-P_2	B_3-P_3	B_4-P_4	B_5-P_1	B_6-P_6	2	$M_z,[\frac{-1}{\sqrt{3}},1,0]^1$
12	B_1-P_5	B_2-P_6	B_3-P_3	B_4-P_4	B_5-P_1	B_6-P_2	1	M_z
13	B_1-P_5	B_2-P_6	B_3-P_4	B_4-P_3	B_5-P_1	B_6-P_2	0	none
14	B_1-P_6	B_2-P_2	B_3-P_3	B_4-P_4	B_5-P_5	B_6-P_1	2	$M_z,[-\sqrt{3},1,0]^1$
15	B_1-P_6	B_2-P_3	B_3-P_2	B_4-P_5	B_5-P_4	B_6-P_1	0	none
16	B_1-P_1	B_2-P_6	B_3-P_5	B_4-P_4	B_5-P_3	B_6-P_2	2	F_x, M_z
17	B_1-P_1	B_2-P_3	B_3-P_2	B_4-P_4	B_5-P_6	B_6-P_5	1	F_y
18	B_1-P_1	B_2-P_2	B_3-P_6	B_4-P_4	B_5-P_5	B_6-P_3	2	$M_z,[\sqrt{3},1,0]^1$
19	B_1-P_2	B_2-P_3	B_3-P_4	B_4-P_5	B_5-P_6	B_6-P_1	3	M_x, M_y, M_z
20	B_1-P_3	B_2-P_4	B_3-P_5	B_4-P_6	B_5-P_1	B_6-P_2	3	M_x, M_y, M_z

Note: Superscript '1' denotes singular force direction in a plane.

4 Numerical simulations

As seen in the previous section, the $6-6$ Stewart Platform with the base and platform of the same size and all legs vertical (configuration No. 1 in Table 1) has force singular direction along X and Y axis and moment singular direction along Z axis. We perturb this configuration so that the Stewart Platform is in a *near-singular* configuration and perform a numerical study to determine the effects of the perturbations. The first set of numerical studies is obtained assuming the joints connecting the legs to the base and platform are spherical. Then we replace the spherical joints by flexural hinges and perform FEA studies to show that the errors due to replacing the spherical joints by flexural hinges are not large. This leads to a preliminary choice of the geometry of the Stewart Platform based sensor sensitive to F_x, F_y and M_z. It may be noted that to get sensitivity in other directions, we have to choose an appropriate configuration from Table 1.

We start by perturbing the symmetry of the connection points in the base and the platform.

Table 2: Nominal geometry of 6-6 Stewart Platform with $\gamma = 33^\circ$

Base coordinates				Platform coordinates			
Point No.	x mm	y mm	z mm	Point No	X mm	Y mm	Z mm
b_1	43.30	25.0	0.0	p_1	41.93	27.23	100
b_2	0	50.0	0.0	p_2	2.616	49.93	100
b_3	-43.30	25.0	0.0	p_3	-44.55	22.70	100
b_4	-43.30	-25.0	0.0	p_4	-44.55	-22.70	100
b_5	0	-50	0.0	p_5	2.616	-49.93	100
b_6	43.3	-25.0	0.0	p_6	41.93	-27.23	100

The half angles, γ and β, between the connection points in the platform and base plates respectively are 30° in the configuration 1 (both the plates are regular hexagons of equal sides). Keeping the half angle in the fixed base, β as 30°, we change platform half angle around the nominal value of 30° from 25° to 35°. Figures 6a & b show the plots of $\det[H]$ and condition number $\text{cond}[H]$ as a function of γ respectively. It can be noted that at $\gamma = 30^\circ$, $\det[H] = 0$. The condition number of $[H]$ (the ratio of the largest to the smallest eigenvalue of $[H]$) falls off from ∞ on both sides of 30°. At $\gamma = 33^\circ$, the condition number is approximately 1910 which is fairly large and we can expect significant magnification[5] in the leg forces for external forces/moment applied along the singular directions F_x, F_y and M_z. Furthermore, the variation in the condition number at $\gamma = 33^\circ$ is not very large (see figure 6c) and one can expect that the magnification will vary less due to expected fabrication tolerances if γ is kept at 33°. The figure 6d shows the variation in the leg forces for γ varying between 31° and 33°. It is observed that the slopes of the curves are small and for a small change in γ about 33°, the change in the slopes is not significant. For the above reasons, we choose $\gamma = 33^\circ$ as the near-singular configuration. The nominal geometry of the Stewart Platform sensor with $\gamma = 33^\circ$ is given in Table 2.

We next perturb the orientation of the platform by rotating about X, Y and Z axis. The figures 7a shows the plot of condition number of $[H]$ due to perturbation of θ_1, θ_2 and θ_3 around the nominal value of 0° respectively. We can observe that the condition number of $[H]$ changes by about 2.5% for θ_1 and θ_2, and for θ_3, the variation is 0.015%, for a variation of $\pm 10^\circ$ about the nominal. Figures 7b and c also shows plots of $\text{cond}[H]$ as a function of distance $|\mathbf{t_z}|$ and $|\mathbf{t_x}|$, and as a function of the base radius R and the platform radius r respectively. We can observe the maximum variation in the condition number for all parameters is less than $\pm 4.5\%$ and the resulting small changes in the leg forces, due to changes in the parameters arising out of tolerances during fabrication and deflection from the applied external force/moment can be accounted for by calibration.

The nominal condition number of $[H]$ is 1910. Since this number is not too high, the force transformation matrix, $[H]$, can be inverted numerically by using a software such as Matlab[25]

[5]We get more magnification in the leg forces if γ is chosen nearer to 30°, but the variation in the condition number is also larger if γ is nearer to 30°.

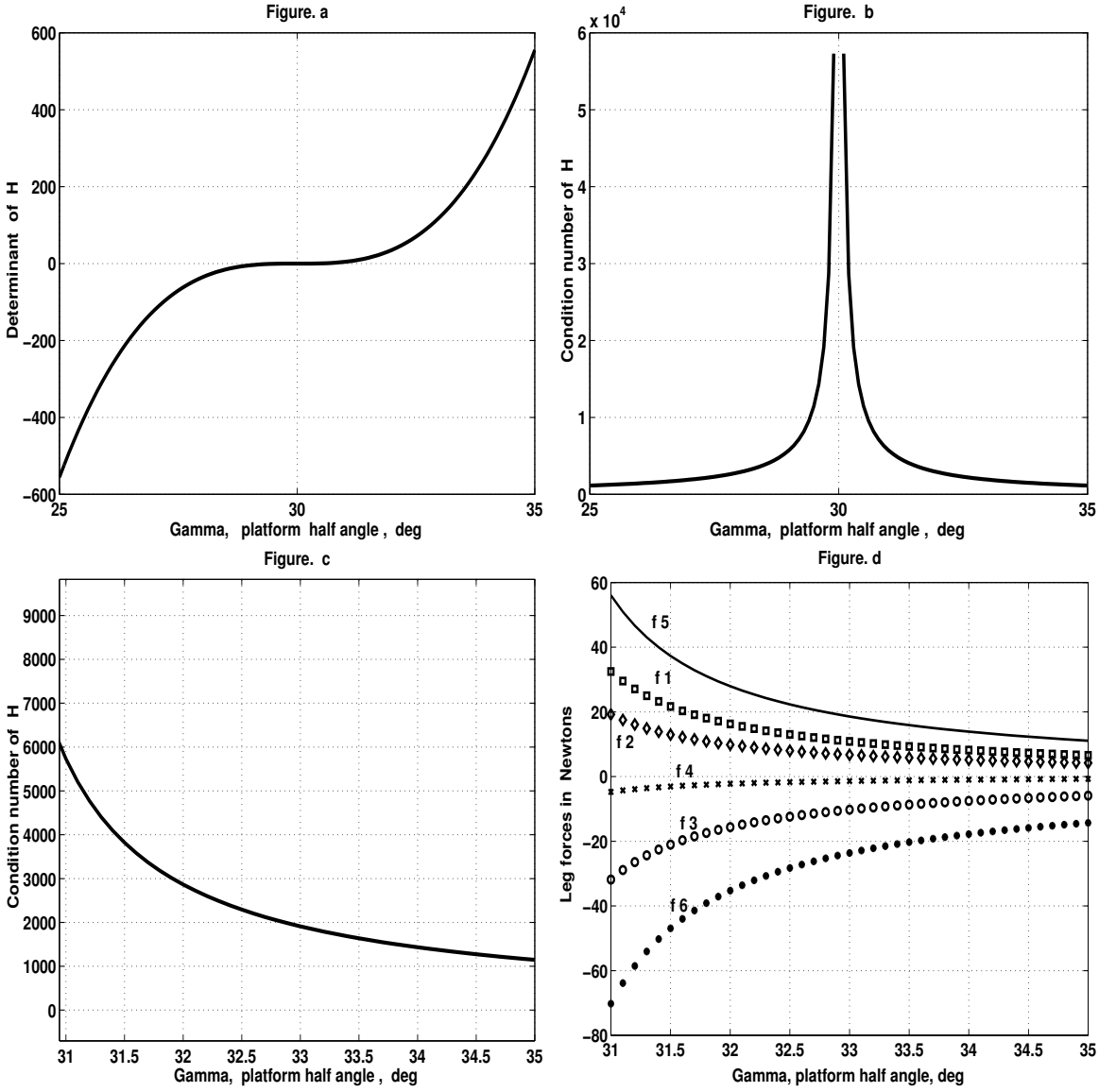

Figure 6: Plot of det$[H]$, Condition No. of $[H]$ and Leg forces with γ

without introducing significant numerical inaccuracy. By inverting $[H]$ we can obtain the leg forces as the external force $\mathbf{F}$ and $\mathbf{M}$ is varied, and numerically verify that we indeed get large magnification in the leg forces. The values of the leg forces for forces/moments acting along X, Y and Z axes are shown in Table 3. We can observe in rows 1, 2 and 6 that there is significant magnification for F_x, F_y and M_z with at least some leg forces being large, and these large leg forces can be measured by strain gages. From row 7, we can also see that when the forces and moments as applied in rows 1 to 6, act together on the platform, the leg forces show superposition of the corresponding values in the leg forces. Finally, figures 8 and 9, show 3D plots of six leg forces as the direction of the applied force and moment are varied. In figure 8 and figure 9, 'al' and 'be' are

the angle the external wrench makes with the X and Y axis fixed to the base. We can observe that the magnification in the leg forces is largest along the singular directions X and Y for force in figure 8 and about Z for moment in figure 9. Orthogonal to the singular directions, there is no magnification.

4.1 Numerical simulations – FE analysis

In the previous numerical simulations, we assumed that the joints of the Stewart Platform are spherical. As done for the planar truss in section 2, we replace the spherical joints with flexural hinges and perform an FE analysis to show that the force magnification in legs occurs even when the joints are replaced by flexural hinges.

The nominal 6-6 configuration was modeled for finite element analysis in software package NISA[23]. The top and bottom plates and the ring sensor are modeled with plate elements. The legs are modeled with 3D beam elements. Each leg is initially divided into twenty elements of 5

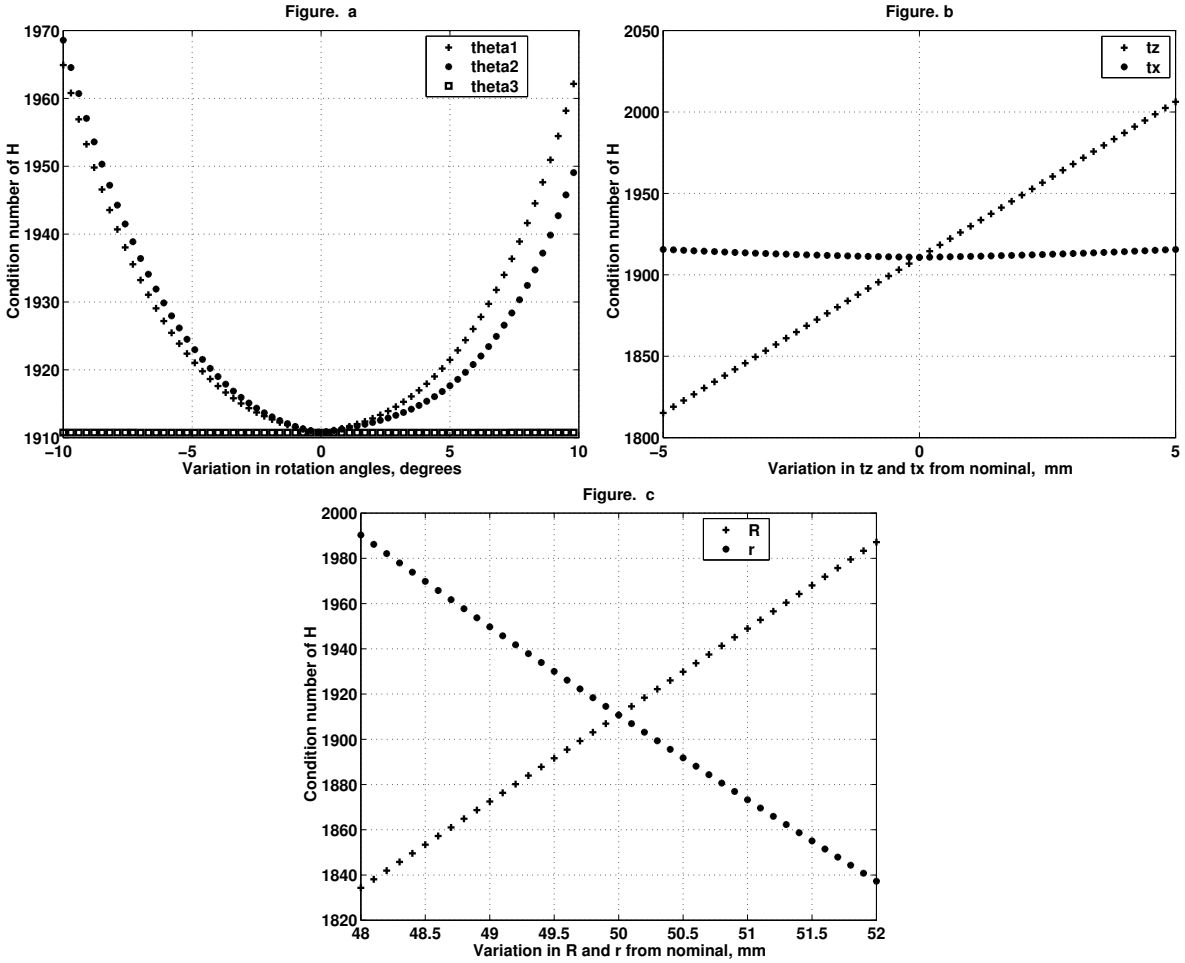

Figure 7: Plot of Condition No. of $[H]$ with respect to parameters

Table 3: Leg forces for external forces/moments acting at the platform centre

	External Loading(N & N-mm)						Leg Forces(N)					
	F_x	F_y	F_z	M_x	M_y	M_z	F_1	F_2	F_3	F_4	F_5	F_6
1	0.98	0	0	0	0	0	-6.808	12.483	-5.675	-5.675	12.483	-6.808
2	0	0.98	0	0	0	0	10.484	-0.654	-11.138	11.138	0.654	-10.484
3	0	0	0.98	0	0	0	0.164	0.164	0.164	0.164	0.164	0.164
4	0	0	0	49.05	0	0	0.171	0.327	0.156	-0.156	-0.327	-0.171
5	0	0	0	0	49.05	0	-0.279	-0.009	0.287	0.287	-0.009	-0.279
6	0	0	0	0	0	49.05	6.250	-6.250	6.250	-6.250	6.250	-6.250
7	0.98	0.98	0.98	49.05	49.05	49.05	9.982	6.061	-9.955	-0.492	19.216	-23.829

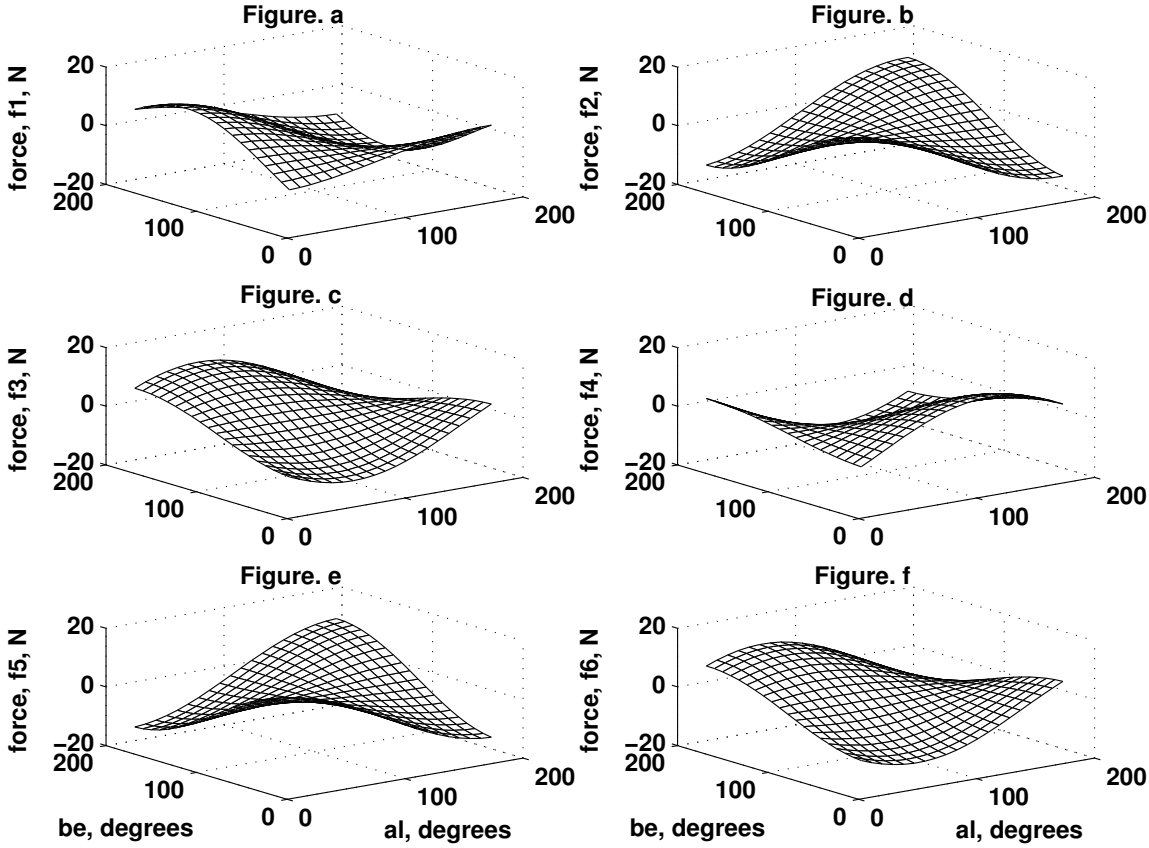

Figure 8: Leg forces versus 'al' and 'be' - only forces applied

mm each. Further, three elements on either end of each leg (at the place of the flexural hinge) are re-meshed with ten elements each. Since, the kink is at the interface of the base and the platform with the legs, the two elements which form the kinked length of 1.0 mm are further meshed to five

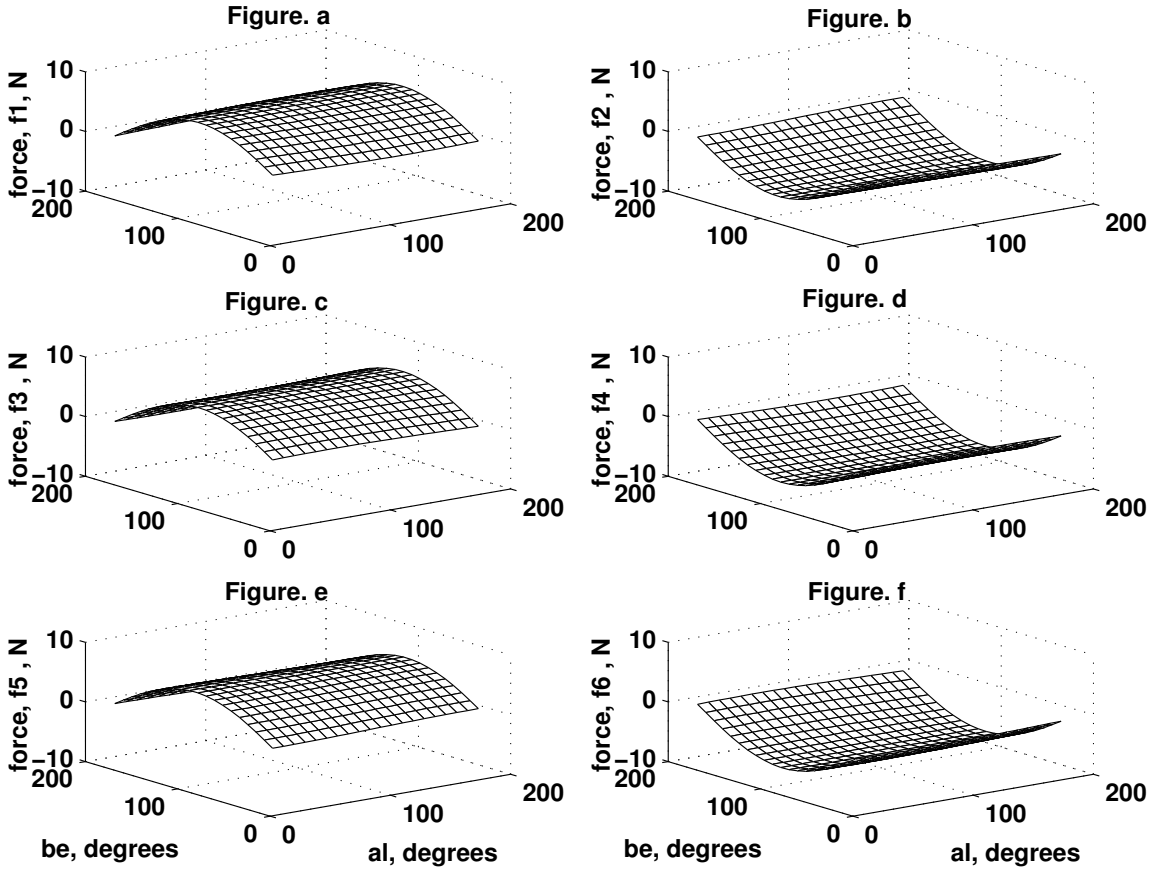

Figure 9: Leg forces versus 'al' and 'be' - only moments applied

elements each, thus providing a graded mesh. The diameter of the beam is 6 mm. The platform has been modeled with plate elements of thickness 5 mm and the rings with plate elements of thickness 2 mm in the plane of the ring. The material chosen for the legs is Titanium alloy (Ti-6Al-4V) for high strength with a Young's modulus of 112000 N/mm^2 and a Poisson's ratio of 0.3. The material chosen for the base and the platform is an Aluminum alloy (for lower self weight) with an Young's modulus of 70000 N/mm^2 and a Poisson's ratio of 0.3. The boundary conditions to the base points at which the sensor is fixed to the ground are assigned zero displacement ($U_x = U_y = U_z = 0$) and zero rotation boundary ($R_x = R_y = R_z = 0$) conditions. The top and bottom end of the legs are node merged to the platform and base respectively. The interface of the plate elements with the beam elements are provided with small diameter beam elements with node merging so that the plate elements can effectively transmit the twist moment about the axis perpendicular to the plane of the plate elements. The FE model has totally 25400 degrees of freedom.

The external loads, applied at the centre of the platform, are $F_x = F_y = F_z = 0.98$ N and $M_x = M_y = M_z = 49.05$ N $-$ mm. The resulting FE model is analyzed and the leg forces in the elements at the middle of the legs, between the platform and the ring sensor, are presented in Table 4. We can observe from Table 4 that, as the kink diameter decreases, the axial forces in the legs

Table 4: Axial forces in the legs

Leg No	Sph. Joint Matlab results	Flexure joints(Kink dimension in mm)							
		No kink	dia 3	dia 2	dia 1	dia 0.75	dia 0.5	dia 0.25	Square 0.5
	N	N	N	N	N	N	N	N	N
1	9.982	-0.2580	-0.1785	0.1354	3.3344	5.9262	8.5681	9.6099	7.9461
2	6.061	0.1501	0.1432	0.1236	0.8741	2.4937	4.8187	5.9468	4.1948
3	-9.955	0.7122	0.7004	0.6416	-1.1792	-3.9858	-7.7587	-9.4902	-6.7679
4	-0.492	0.6426	0.5994	0.4356	-0.7083	-1.0261	-0.8888	-0.7711	-0.9722
5	19.216	0.3885	0.5082	0.9967	6.4687	11.3943	16.6858	18.9362	15.4066
6	-23.829	-0.6543	-0.7917	-1.3528	-7.8097	-13.8213	-20.4431	-23.2497	-18.8254

Table 5: Forces and moments in the legs from FE analysis

Leg no.	Spherical Joints	Flexure Joints					
	Matlab Results	FE analysis results from NISA					
	Leg Forces N	F_x N	F_y N	F_z N	M_x N-mm	M_y N-mm	M_z N-mm
f_1	9.982	7.946	0.030	-0.051	0.230	-1.250	-0.744
f_2	6.061	4.195	0.018	0.044	0.275	0.814	-0.418
f_3	-9.955	-6.768	-0.032	0.015	0.263	0.304	0.824
f_4	-0.493	-0.972	-0.002	-0.050	0.229	-1.266	0.015
f_5	19.216	15.407	0.057	0.047	0.272	0.761	-1.429
f_6	-23.829	-18.825	-0.071	0.012	0.264	0.367	1.759

approach the value obtained from statics (see column 1 in Table 4) and row 7 in Table 3 with spherical joints. It can be observed that the transverse forces and moments become small and the axial forces dominate. Though the axial forces in the case of the kink diameter 0.25 mm are closer to numerical results obtained with spherical joints as shown in Table 4, from manufacturing point of view, the kink diameter with 0.5 mm is more appropriate. For ease of fabrication, the hinge was chosen to be 0.5 mm square and the axial forces for this geometry are also shown in Table 4. Further, for the case of kink diameter of 0.5 mm, all the forces and moments acting on the node near the middle of the legs are presented in Table 5. It can be observed that 0.5 mm square hinge elements being slightly stiffer, give slightly smaller axial forces. FE analysis using in NISA[23] (see figures 12 and 13) shows that the maximum stress was around 295 N/mm^2, in the flexural hinge region, in legs 5 and 6. This value of stress is far away from the yield value of 880 N/mm^2 for the chosen Titanium alloy. The maximum resultant displacement of around 0.5 mm is seen at the leg 5 and leg 6 interfaces. From, the numerical analysis in section 4, the magnification and condition

number do not change much for a displacement of 0.5 mm, and hence is acceptable. Hence, 0.5 mm square is chosen for the flexural hinge in the Stewart Platform based sensor.

The FE model was used to obtain the natural frequencies of the designed sensor with the mass of the platform as 0.1425 kg and the mass of each leg as 0.0151 kg. Three modes were evaluated and the first, second and the third natural frequencies are found to be 22.4 Hz for translational mode along the Y direction, 22.7 Hz for the translational mode along the X direction and 46.0 Hz for the rotational mode about the Z axis of the sensor, respectively. Hence the sensor is more or less equally sensitive about the X and Y axes and more stiff for rotation about the Z axis. This is expected because the flexure joint is stiffer in torsion than in bending. In addition, the maximum displacements (for the load used to obtain Table 4) along X and Y were found to be less than 0.5 mm and less than 0.05 mm along Z. Thus, the natural frequencies and the displacements indicate that the sensor is reasonably stiff in the sensitive directions.

5 Design of the force-torque sensor

We first start with the design of one of the legs in the $6-6$ Stewart Platform based sensor. The aim is to obtain largest possible sensitivity for a given axial load in a leg.

5.1 Design of the sensing element in the leg

A number of options were considered[16, 32, 34] and a ring type section, shown in figure 10, was studied in detail. The strain gages are to be mounted on the outside and inside of the walls, near the centre, in the longitudinal directions. For a stiff sensor, it is desirable that the deflection be as low as possible. At the same time, the strain in the sensing element should be adequately measurable over the intended range of operation of the sensing element.

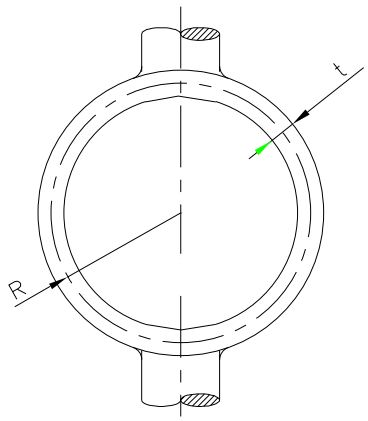

Figure 10: Schematic of the sensing element

The geometry of the sensing element is determined by the mean radius R, the width b (perpendicular to the plane of the paper), and the thickness t. The empirical expressions for bending

moment, strain and deflection for an applied load P are given in Roark[33]. The expression for the maximum bending moment M at central plane is

$$M = -0.1817PR \tag{14}$$

The strain due to this moment is $\frac{My}{EI}$ where E is the Young's modulus of the material. The deflection under load P, denoted by δ is given by

$$\delta = -0.149k\frac{PR^3}{EI} \tag{15}$$

where k is determined by the ratio of the outer to the inner diameter of the ring. For a ratio of 1.3, the factor k is 1.03 (see Roark[33] for details).

From the numerical simulation in section 4, (see Table 3 row 7), it can be observed that for a loading of $F_x = F_y = F_z = 0.98$ N and $M_x = M_y = M_z = 49.05$ N $-$ mm on the centre of the platform, the maximum force of approximately -23.54 N is seen in leg no. 6. It was observed that, if F_x is reversed and all others remain the same, the maximum force turns out to be approximately 23.54 N. Hence, the sensor in the leg is to be designed for an axial load of approximately 30 N. The goal is to choose the geometry such that the strain is maximum and the deflection under the load is minimum. It was found from the formulas that, for a mean radius R of 9 mm, thickness t of 2mm and width b of 5 mm, the strain ϵ is approximately 125 micro-strain. The vertical deflection for the same load and geometry is 0.01 mm. This chosen nominal configuration is modified with a flat portion of 6 mm at the leg-ring junction for ease of fabrication. This modified configuration was also modeled in FEM and the displacement was found to be 0.00946 mm. It was also verified that the stress (and consequently strain) near the central region was nearly constant so that the strain gages could be mounted in that region.

The material considered for the sensor is Titanium alloy (Ti-6Al-4V alloy) as it has a low E which increases the strain value thus improving the sensitivity of the sensor. From the FE analysis it is found, that for a nominal axial load of 30 N in compression and for the chosen geometry, the strain is approximately 145 micro-strains (compressive) at the inside surface of the ring and 110 micro-strains (tensile) at the outside surface of the ring[6]. This would yield approximately 510 micro-strains for a full bridge strain gauge configuration.

5.2 Design of the flexural hinge

As discussed earlier, the flexural hinge was nominally chosen to be 0.5 mm square and 1 mm in length. The leg with the hinge was fabricated by wire cut electro-discharge machining process from a monolithic piece of Titanium alloy. In addition, to provide overload protection against *biaxial bending* and to minimize stress concentration, the hinge was designed as shown in figure 11. The 0.2 mm slit (see Detail C in figure 11) does not allow the hinge to rotate more than approximately 3.8° and the resulting bending stress is far away from the yield stress of 880 N /mm^2 for the Titanium alloy used. As observed from FE analysis, the maximum stress at the flexural hinge of 294 N/mm^2 is about a third of the yield stress.

[6]The average strain is 127.5 micro-strain at the mean radius and matches closely the value of 125 micro-strain from the empirical formula.

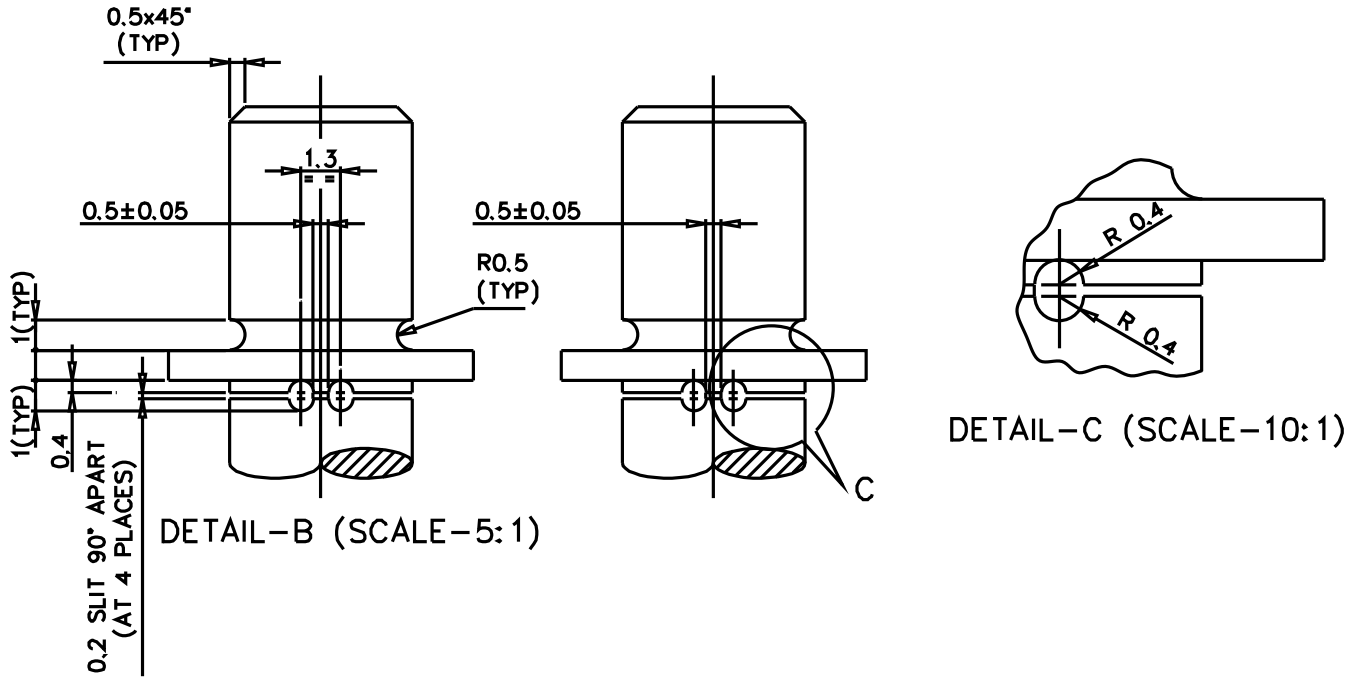

Figure 11: Detailed view of the flexural hinge

5.3 Finite element analysis of the sensor

The overall configuration of the 6-6 Stewart Platform based sensor, sensitive to F_x, F_y and M_z, with flexure hinges and with the sensing element was modeled in NISA as shown in figure 12. The mass of the platform is 0.1425 kg and the mass of each leg is 0.0151 kg. Representative simulation results showing a plot of deflection and the stresses in the structure are shown in figures 12 and 13 respectively. For the externally applied loading of $F_x = F_y = F_z = 0.98$ N, $M_x = M_y = M_z = 49.05$ N-mm, the maximum deformation is obtained to be 0.5 mm and the maximum stress is seen to be about 294 N/mm^2 at the flexible hinges. These are well within the allowable values of deflection of the platform and the maximum allowable stresses in the material.

6 Experimental Results

A prototype of the designed sensor was fabricated and is shown in the figure 14. In this prototype, each leg with the flexible hinges and sensing element, is machined from a single piece of Titanium alloy and were then assembled with the platform and base. Although it is well known that the entire sensor should be monolithic to avoid hysteresis effects, in this prototype the legs are assembled to the platform and base with screws torqued sufficiently to avoid slippages. This is because our aim is to demonstrate sensitivity to external loads in certain directions and hence the externally applied loads are chosen to be low[7] in the sensitive directions. An additional goal is to use the *same legs* for

[7]The extensive experiments done on the prototype, for the range of externally applied loads, did not show any noticeable hysteresis.

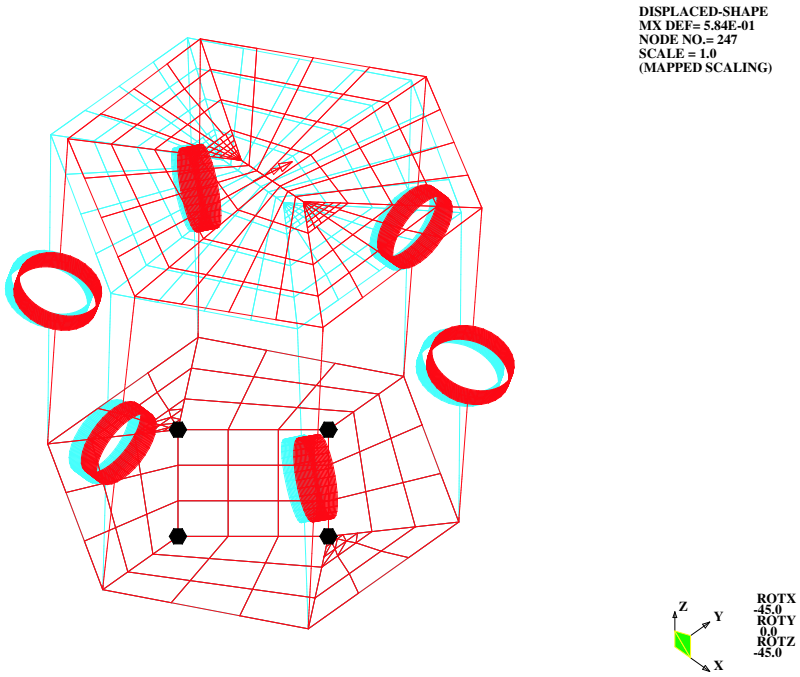

Figure 12: Deflection (mm) of the sensor

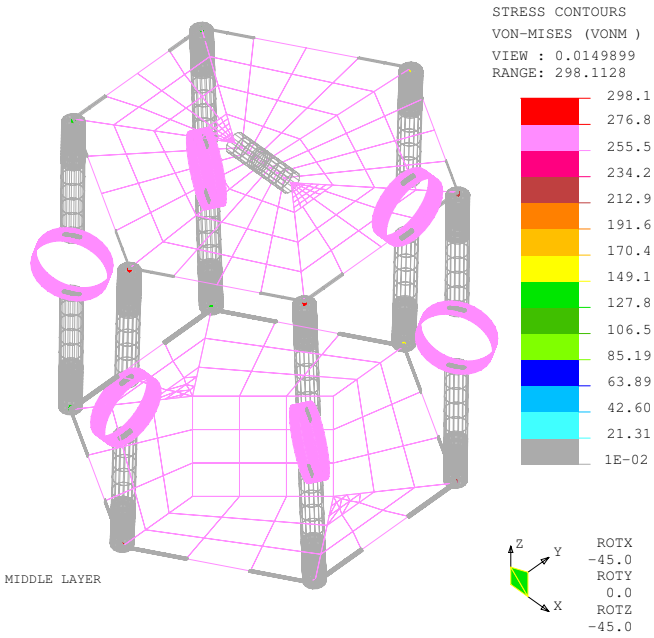

Figure 13: Stress (N/mm^2) in the sensor

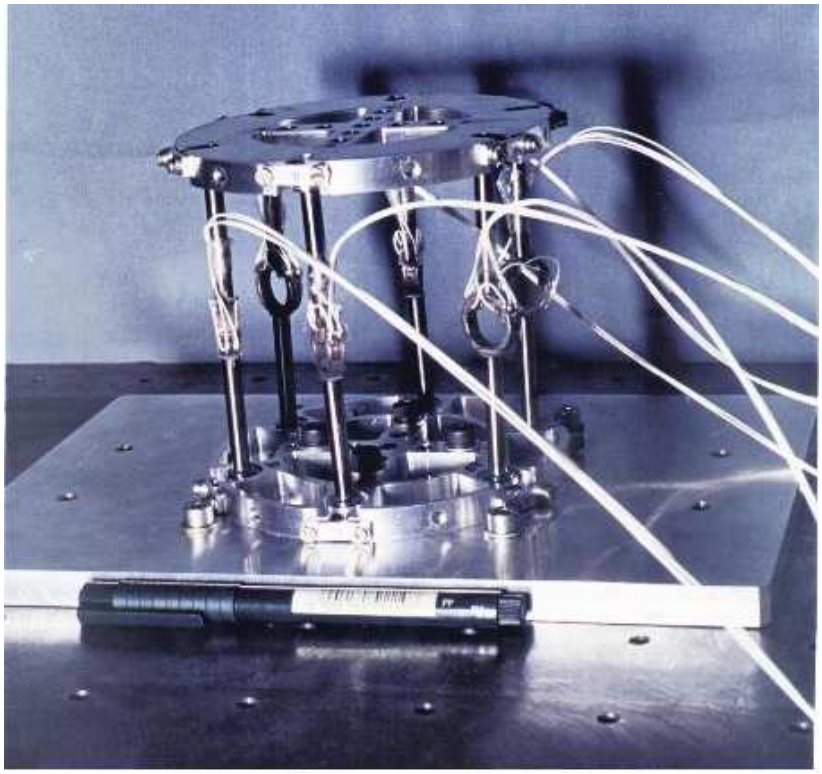

Figure 14: Stewart platform based force-torque sensor

other near-singular Stewart Platform based sensors and demonstrate sensitivity to external loads applied along different directions.

6.1 Calibration of individual legs

Strain gages, with a gauge factor of 2.14, were bonded near the mid-plane of the rings of the Titanium alloy legs in full-bridge configuration resulting in a bridge factor of 4.0. The strains in the legs were measured by a calibrated P3500 Measurement Group strain indicator with an amplification setting of approximately 10,000 μstrain/ Volt. Each of the six legs was mounted in a specially designed fixture and calibrated with loads up to 61.80 N in tension. Table 6 shows calibration factors, standard deviation and maximum deviation of the legs. The loading and unloading were done in steps and it was observed that the behavior was almost linear with no hysteresis.

6.2 Response to external loading

The sensor was loaded externally, in a specially designed fixture, by means of standard dead weights. The loading and unloading along the sensitive directions, namely F_x, F_y and M_z, was done in steps and limited to 0.98 N and 49.05 N-mm respectively. The results for F_x, F_y and F_z are shown in figure 15. The results for M_x, M_y and M_z are shown in figure 16. The experimental data was compared with numerical results obtained from FE analysis, and it was observed that the

Table 6: Calibration factors of legs

Leg No.	Calib. Const. (μ strain/N)	Intercept (μ strain)	Std. deviation (μ strain)	Abs. Max. deviation (μ strain)
1	13.786	0.303	0.444	1.097
2	13.958	1.179	0.496	1.179
3	14.102	0.059	0.481	1.150
4	13.921	2.047	0.683	2.047
5	13.994	1.237	0.667	1.237
6	14.046	-0.457	0.775	2.457

maximum error between the numerical and experimental data is less than 10% in the sensitive directions. From the experimental data in figures 15 and 16, one can clearly see that the sensor is sensitive to F_x, F_y and M_z and *not* to F_z, M_x and M_y.

6.3 Calibration of sensor and measurement of applied load

The experimental data shown in figures 15 and 16 was used to determine the force transformation matrix, $[H]$, as follows:

We recall from equation (9) that $(\mathbf{F};\mathbf{M})^T = [H]\mathbf{f}$. The first component of the applied external load, F_x, can be re-written as

$$F_x = f_1 H_{11} + f_2 H_{12} + f_3 H_{13} + f_4 H_{14} + f_5 H_{15} + f_6 H_{16} \tag{16}$$

where $f_i,\ i = 1,..,6$ are the measured leg forces and $H_{1j},\ j = 1,..,6$ are the unknown elements of the first row of $[H]$ – these are also the first row of the calibration matrix $[H]$. We take several data points, with known F_x values which could be positive, negative or zero, from the experimental data shown in figures 15 and 16, and rearrange equation (16) as

$$\begin{pmatrix} F_{1x} \\ F_{2x} \\ . \\ . \\ F_{nx} \end{pmatrix} = \begin{bmatrix} f_{11} & f_{12} & f_{13} & f_{14} & f_{15} & f_{16} \\ f_{21} & f_{22} & f_{23} & f_{24} & f_{25} & f_{26} \\ . & . & . & . & . & . \\ . & . & . & . & . & . \\ f_{n1} & f_{n2} & f_{n3} & f_{n4} & f_{n5} & f_{n6} \end{bmatrix} \begin{pmatrix} H_{11} \\ H_{12} \\ H_{13} \\ H_{14} \\ H_{15} \\ H_{16} \end{pmatrix} \tag{17}$$

Denoting the $n \times 6$ matrix on the right-hand side by $[f]$, we can obtain $H_{1j},\ j = 1,..,6$ as

$$(H_{1j}, H_{2j}, H_{3j}, H_{4j}, H_{5j}, H_{6j})^T = [f]^{\#}(F_{1x}, F_{2x}, ..., F_{nx})^T \tag{18}$$

where $[f]^{\#}$ is the pseudo-inverse of $[f]$.

The above method is used to compute all the rows of the $[H]$ matrix, and for 25 data points chosen from the experimental test data, we obtain

$$[H] = \begin{bmatrix} -0.0195 & 0.0279 & -0.0266 & -0.0223 & 0.0369 & -0.0117 \\ 0.0287 & -0.0076 & -0.0368 & 0.0280 & 0.0036 & -0.0272 \\ 0.8890 & 0.8294 & 0.8321 & 0.8845 & 0.9704 & 0.9712 \\ 22.7237 & 44.3631 & 21.0266 & -18.6015 & -45.1386 & -26.4990 \\ -6.7289 & -5.5169 & -5.0906 & -4.8826 & -5.1129 & -6.4894 \\ 1.3319 & -1.5084 & 1.8969 & -1.4110 & 1.2823 & -1.9917 \end{bmatrix} \tag{19}$$

It may be noted that the condition number of the computed $[H]$ matrix is approximately 1351.8 as compared to 1910 obtained for the force transformation matrix with spherical joints. The above $[H]$ matrix can be used for 3D force-torque measurements by multiplying $[H]$ with the leg-forces obtained from the measured strain readings. We present two sample cases.

- For a combined 3D external loading of $(0.9123, 0.9123, 0)^T$ N force and $(-10.0356, 10.03560, 0)^T$ N-mm moment, the measured values of forces and moments are $(0.9270, 0.8819, 0.0265)^T$ N and $(-13.0081, 10.1789, -1.4352)^T$ N-mm respectively. It may be noted that the FEA computed values for the externally applied 3D loading are $(0.9241, 0.8809, 0.0932)^T$ N of force and $(-19.2041, 12.3772, -0.5258)^T$ N-mm.

- For a combined 3D loading of $(0.9123, 0.9123, 0)^T$ N force and $(-10.0356, 10.0356, -45.6165)^T$ N-mm moment, the measured values of forces and moments are $(0.8937, 0.9153, 0.1462)^T$ N and $(-12.2085, 8.9987, -45.9569)^T$ N-mm respectively. The computed FEA values for the 3D loading is $(0.8780, 0.9261, 0.2688)^T$ N force and $(-21.8783, 18.0896, -43.7448)^T$ N-mm moment.

We can make the following observations:

- The performance of the prototype sensor is very good for sensing forces and moments in the chosen sensitive directions and errors are around 3%. This is because even small forces and moments in the sensitive directions lead to large strain readings in the legs, due to the mechanical magnifications, and they could be more accurately measured with the strain measuring device used.

- A magnification of about 10 is observed in the sensitive directions. One way to increase magnification, up to the value obtained with spherical joints, is to use smaller diameter at the flexure as shown in Table 4. Another approach to increase magnification is to choose the angle γ closer to 30° (see footnote of page 13 and figure 6). However, both these approaches are limited by the allowable stress in the chosen material since the stresses in the flexure hinge increases and as a result the maximum external load that can be measured decreases.

- The performance of the prototype sensor in the non-sensitive directions is less accurate. This is due to the low strain readings observed for several calibration tests – for F_z loading on the platform, at least 0.49 N was required to produce measurable strain. A strain measuring device with larger electronic amplification is planned to be used for more detailed calibration in the future.

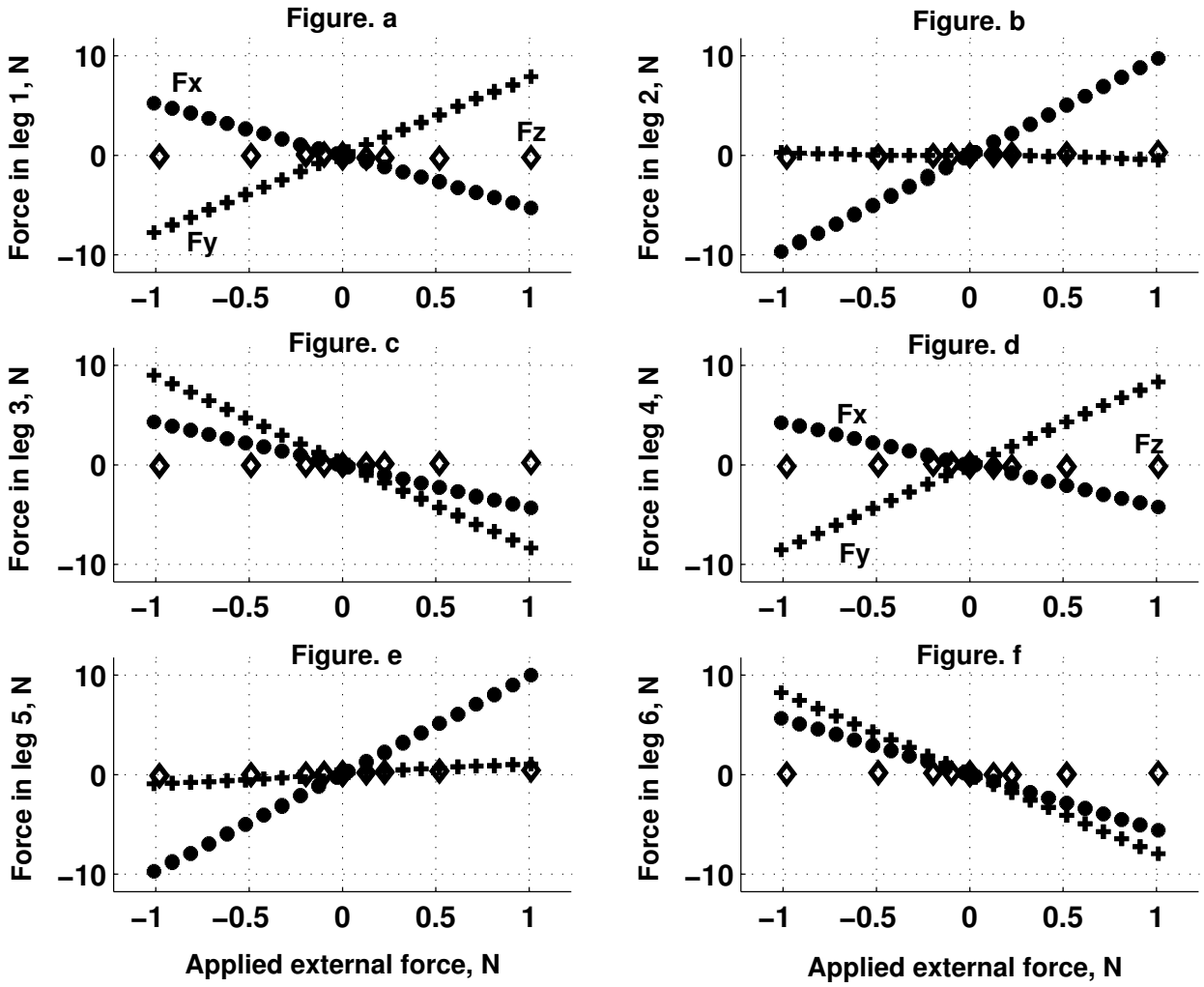

Figure 15: Experimental data for applied external force

- The computed FEA values are in general larger. This is expected since FE based models are known to be stiffer.

7 Conclusions

This paper deals with the analysis and design of a Stewart Platform based force-torque sensor in a *near-singular* configuration. It is first shown analytically, with a simple planar truss near a singular configuration, that force applied in a singular direction gives large forces in the truss members. It is also shown that replacing rotary joints with flexible hinges does not significantly alter the magnification of forces in the members. Flexible hinges avoid friction, backlash and other unpredictable non-linearities associated with mechanical joints. These two key ideas are then used to develop a novel force-torque sensor based on a Stewart Platform at a near-singular configuration.

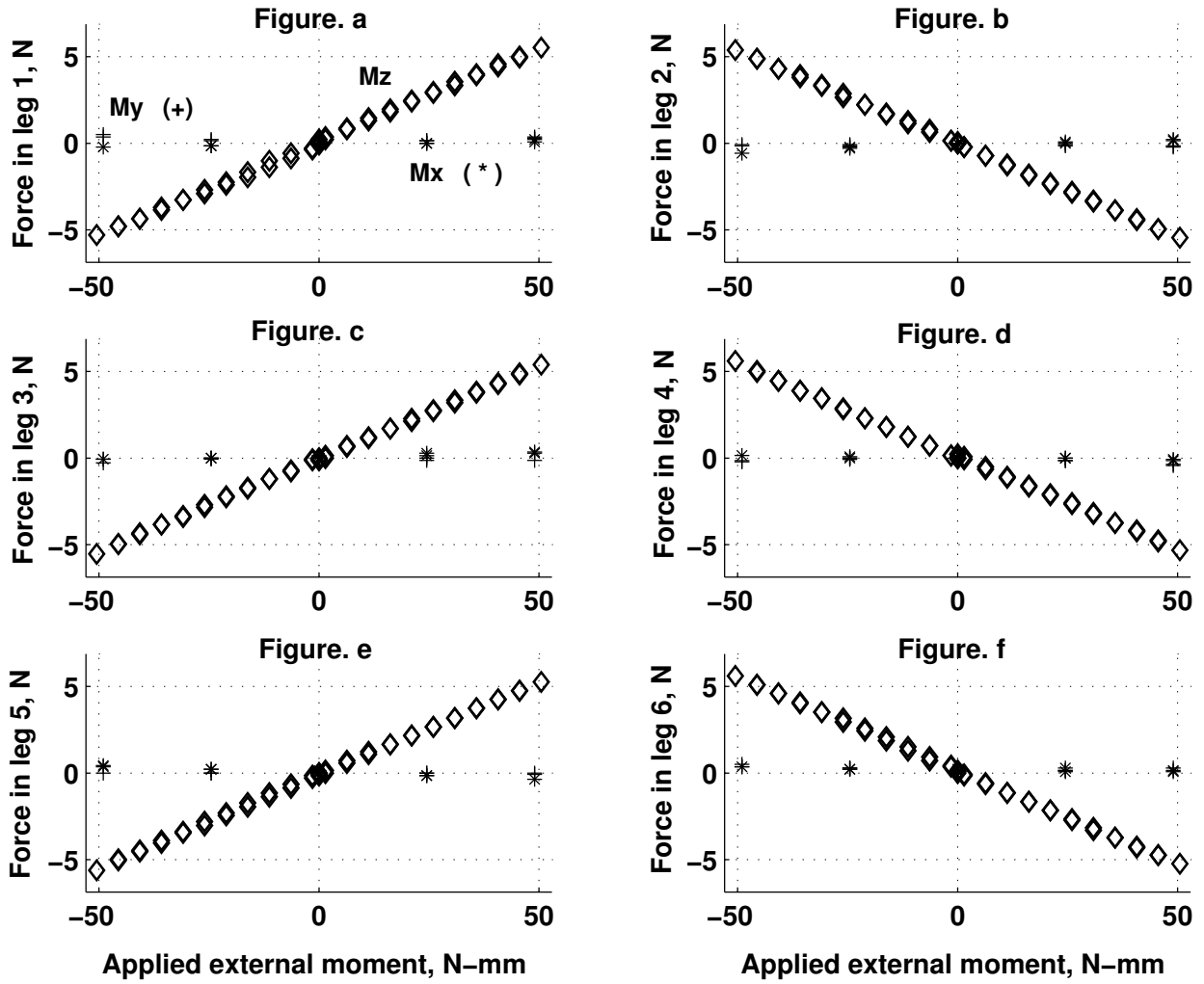

Figure 16: Experimental data for applied external moment

It is first shown that various singular configurations can be obtained to get high sensitivity to various combinations of the six components of force and torque. One such configuration where the sensitivity of force is in the $X-Y$ plane and moment about the Z direction is then taken up for detailed analysis and a nominal configuration for the sensor is obtained. Then, we design a sensing element, by numerical computations and FEA, which can give adequate response for a chosen range of applied forces and moments on the platform. The flexure joint has been configured for overload protection in biaxial bending. A prototype of the Stewart Platform based sensor was fabricated and experimental results clearly demonstrate the sensitivity to the externally applied forces and moment in the $X-Y$ plane and along Z direction respectively. From the experimental results, we obtain the force transformation matrix, and this is used to demonstrate 3D force-torque measurement.

Acknowledgments

The authors wish to thank Sandipan Bandyopadhyay for help in using Mathematica package and Badari Narayana, K., ISRO Satellite Centre, for help in using NISA package. The authors also wish to thank Nageswara Rao, M. and Sridhara, C. D., of Spacecraft Mechanisms Group, ISRO Satellite Centre, Bangalore, for their encouragement in this work.

References

[1] Stewart, D., A platform with six degrees of freedom, *Proc. of Institution of Mechanical Engineers*, Part 1, Vol. 180(15), 1965, pp. 371-386.

[2] Hunt, K. H., *Kinematic Geometry of Mechanisms*, Clarendon Press, Oxford, 1978.

[3] Fichter, E. F., The Stewart Platform manipulator: general theory and practical construction, *Int. Journal of Robotics Research*, Vol. 5, No. 2, 1986, pp. 157-182.

[4] Portman, V. T., Sandler, B. and Zahavi, E., Rigid 6x6 parallel platform for precision 3-D micro-manipulation: theory and design application, *IEEE Trans. of Robotics and Automation*, Vol. 16, No.6, 2000, pp. 629-643.

[5] Gaillet, A. and Reboulet, C., A isostatic six component force and torque sensor, *Proc. of the 13 Int. Conf. on Industrial Robotics*, 1983, pp. 18.102-18.111.

[6] Rees Jones, J., Cross coordinate control of robot manipulators, *Proc. of the Int. Workshop on Nuclear Robotic Technologies*, 1987.

[7] Kerr, D. R., Analysis, properties and design of Stewart Platform transducer, *Trans. ASME Journal of Mechanisms, Transmissions and Automation in Design*, Vol. 111, 1989, pp. 25-28.

[8] Nguyen, C. C., Antrazi, S. S and Zhen Lie Zhou., Analysis and implementation of six degrees of freedom Stewart Platform based force sensor for passive compliant robotic assembly, *Proc. of IEEE Southeast Conf.*, 1991, pp. 880-884.

[9] Romiti, A. and Sorli, M., Force and moment measurement system on a robotic assembly hand, *Sensors and Actuators A*, Vol. 32, 1992, pp. 531-538.

[10] Sorli, M. and Zhmud, N., Investigation of force and moment measurement system for a robotic assembly hand, *Sensors and Actuators A*, Vol. 37-38, 1993, pp. 651-657.

[11] Hongrui, W., Feng, G. and Huang Zhen, H., Design of six axis force/torque sensor based on Stewart Platform related to isotropy, *Chinese Journal of Mechanical Engineering*, Vol. 3, 1998.

[12] Dasgupta, B., Reddy, S. and Mruthyunjaya, T. S., Synthesis of a force-torque sensor based on the Stewart Platform mechanism, *Proc. National Convention of Industrial Problems in Machines and Mechanisms (IPROMM'94)*, Bangalore, India, pp. 14-23.

[13] Hirose, S., and Yoneda, K., Development of optical 6-axial force sensor and its signal calibration considering non-linear interference, *Proc. IEEE Intl. Conf. Robotics and Automation*, 1990, pp. 46-53.

[14] Hirzinger, G., and Dietrich, J., Multi-sensory robots and sensor based path generation, *Proc. IEEE Intl. Conf. on Robotics and Automation*, 1986, Vol. 3, pp. 1992-2001

[15] Paros, J. M. and Weisbord, L., How to design flexure hinges, *Machine Design*, 1965, pp. 151-156.

[16] Abe, K., Miwa, T. and Uchiyama, M., Development of a 3 axis planar force/torque sensor for very small force/torque measurement, *JSME International Journal*, Series C, Vol. 12, No. 2, 1999, pp. 376-382.

[17] McInroy, J. E. and Hamann, J. C., Design and control of flexure jointed hexapods, *IEEE Trans. of Robotics and Automation*, Vol. 16, No. 4, 2000, pp. 372-381.

[18] Zhang, S. and Fasse, E. D., A finite-element-based method to determine the spatial stiffness properties of a notch hinge, *Journal of Mechanical Design*, Vol. 123, 2001, pp. 141-147.

[19] Champagne, P. J., Cordova, S. A., Jacoby, M. S. and Lorell, K. R., Development of a precision six axis laboratory dynamometer, *NASA-CP-3147, 26th Aerospace Mechanisms Symposium*, 1992, pp. 331-348.

[20] Gosselin, C. and Angeles, J., Singularity analysis of closed loop kinematic chains, *IEEE Trans. of Robotics and Automation*, Vol. 6, No. 3, pp. 281-290, 1990.

[21] Basu, D. and Ghosal, A., Singularity analysis of platform-type multi-loop spatial mechanisms, *Mechanism and Machine Theory*, Vol. 32, No. 3, 1997, pp. 375-389.

[22] Srinath, L. S., *Advanced Mechanics of Solids*, Tata McGraw-Hill Publishing Company, New Delhi, 1983.

[23] *NISA II/DISPLAY III Users Manual*, Engineering Mechanics Research Corporation, USA, Version 7, 1997.

[24] Ranganath, R., *Analysis and design of a near-singular Stewart Platform based force-torque sensor*, Ph. D. Thesis, M.E. Dept., IISc Bangalore, May 2003.

[25] *MATLAB Users Manual*, Mathworks Inc., USA, 1992.

[26] Wolfram, S., *The Mathematica*, Cambridge University Press, Third Edition, 1996.

[27] Ghosal, A. and Ravani, B., A differential-geometric analysis of singularities of point trajectories of serial and parallel manipulators, *Trans. of ASME, Journal of Mechanical Design*, Vol. 123, 2001, pp. 80-89.

[28] Merlet, J. P., Singularity configurations of parallel manipulators and Grassman geometry, *Int. Journal of Robotics Research*, Vol. 8, No. 5, 1989, pp. 45-56.

[29] Ball, R. S., *A Treatise on The Theory of Screws*, Cambridge University Press, Cambridge, 1900.

[30] Roth, B., Screws, motors and wrenches that cannot be bought in a hardware store, *Robotics Research: The First International Symposium, M. Brady and R. Paul(Eds.)*, pp. 679 - 693, 1984

[31] Sandipan, B., Study of singularities in parallel manipulators and closed-loop mechanisms, *M. E. Thesis*, IISc Bangalore, 2000.

[32] Dwarakanath, T. A., Dasgupta, B. and Mruthyunjaya, T. S., Design and development of a Stewart Platform based force-torque sensor, *Mechatronics*, Vol. 11, 2001, pp. 793-809.

[33] Roark, R. J., *Formulas for Stress and Strain*, 4th Edition, McGraw-Hill Book Company, 1965.

[34] Gorinevsky, D. M., Formalsky, A. M., and Schneider, A. Y., *Force Control of Robotics Systems*, CRC Press, New York, 1997.